A Facility Effect Characterization Test of the BHT-6000 Hall Thruster

Wensheng Huang[1],
National Aeronautics and Space Administration Glenn Research Center, Cleveland, OH, 44135, USA

James H. Gilland[2],
Ohio Aerospace Institute, Cleveland, OH, 44135, USA

Daniel A. Herman[3],
National Aeronautics and Space Administration Glenn Research Center, Cleveland, OH, 44135, USA

Lucy Zuo[4], Charlie Feng[5], Peter Wright[6], Ian Johnson[7]
Maxar Space Systems, Palo Alto, CA, 94303, USA

Carl Mullins[8], Kurt Hohman[9]
Busek Company Inc., Natick, MA, 01760, USA

During the development of the BHT-6000 Hall thruster for flight on NASA's Power and Propulsion Element, a facility effect test campaign was performed on an engineering unit of the thruster. Testing occurred in Vacuum Facility 5 at NASA Glenn Research Center. The goal of the test campaign was to characterize the behavior of the BHT-6000 Hall thruster as functions of facility effects such that the thruster's in-flight behavior can be reasonably bounded. In particular, the behavior of the thruster with regard to the background pressure and electrical environment was tested. The background pressure was controlled by injecting supplemental propellant flow into the environment, while the electrical environment was controlled by biasing the facility beam dump. Thrust was found to remain constant over the tested range of pressures while specific impulse was found to increase slightly (1 to 1.5% over a range of up to 20 μTorr, depending on operating point). Plasma plume properties, particularly of ions exiting the side of the thruster, were found to be highly sensitive to pressure and may require pressures of less than a few μTorr for accurate measurements. The

[1] PPE NASA 6kW Thruster Insight Lead, Electric Propulsion Systems Branch, AIAA Associate Fellow, wensheng.huang@nasa.gov.
[2] Senior Scientist, Electric Propulsion Systems Branch, AIAA Associate Fellow.
[3] PPE NASA Ion Propulsion Subsystem Manager, Electric Propulsion Systems Branch, AIAA Associate Fellow.
[4] Lead Test Engineer, Propulsion Engineering, AIAA member.
[5] Thruster Responsible Engineer, Propulsion Engineering, AIAA member.
[6] Electric Propulsion Engineer, Propulsion Engineering, AIAA member.
[7] Lead Subsystem Engineer, Propulsion Engineering, AIAA member.
[8] BHT Engineer, AIAA member.
[9] BHT Program Manager, AIAA member.

thruster was found to operate identically with changing beam dump bias voltage to within measurement uncertainties.

I. Abbreviations

CMV	=	Co-Manifested Vehicle	LP	=	Langmuir Probe
ESDMD	=	Exploration Systems Development Mission Directorate	OP	=	Operating Point
			PPE	=	Power and Propulsion Element
FP	=	Faraday Probe	RPA	=	Retarding Potential Analyzer
GRC	=	Glenn Research Center	VF5	=	Vacuum Facility 5
HALO	=	Habitation and Logistics Outpost	WFS	=	Wien Filter Spectrometer

II. Introduction

NASA, under the Artemis program, is building Gateway, a Moon-orbiting outpost that provides support for sustainable, long-term human exploration of the lunar surface and serves as a steppingstone to exploration of Mars. The first two elements of the Gateway are the Power and Propulsion Element (PPE) and the Habitation and Logistics Outpost (HALO), and they will be launched together as the co-manifested vehicle (CMV) [1]. NASA has partnered with Maxar Space Systems to build the PPE while leveraging existing commercial spacecraft platform and technical expertise. The PPE will utilize a 48-kW electric propulsion system comprised of three 12-kW Hall thrusters and four 6-kW Hall thrusters [2] (not all thrusters are operated simultaneously).

The four 6-kW Hall thrusters are BHT-6000s supplied by the Busek Co. Inc. of Natick, MA. As a part of the engineering development of the BHT-6000, a facility effect characterization test campaign was performed on an engineering unit at NASA Glenn Research Center (GRC). The goal of the test campaign was to characterize the behavior of the BHT-6000 Hall thruster as functions of facility effects so that the in-flight behavior of the thruster can be approximated. For the background pressure test, the background pressure was varied by injecting propellant into the far-field of the thruster and measuring the thruster's characteristics. For the electrical environment test, the beam dump was biased to a range of voltages that may be encountered in the space environment and measuring the thruster's characteristics. The obtained data will a support a variety of activities including mission design, planning of spacecraft operations, and analysis of plume-induced erosion of various spacecraft components.

This paper will describe the test setup, analysis method, and test results for the aforementioned facility effect characterization test.

III. Experimental Setup

A. Thruster and Test Matrix

The test article is a BHT-6000 Hall-effect thruster supplied by the Busek Co. Inc. of Natick, MA. Fig. 1 shows the BHT-6000 engineering unit installed on the thrust stand inside of Vacuum Facility 5 (VF5). This thruster was developed as an upgrade of the BHT-5000 Hall thruster, the development of which was described in a prior publication [3].

Using predictions from erosion modeling, the BHT-6000 magnetic configuration was designed for low erosion. The thruster has a centrally mounted hollow cathode with barium oxide impregnated porous tungsten emitter. The discharge chamber is designed to have high magnetic and electric fields in the discharge and acceleration zone and low magnetic and electric fields near the anode electrode to minimize losses. The propellant distributor was designed to enhance azimuthal flow uniformity. The magnetic circuit consists of one inner coil and four outer coils and was designed to generate a magnetic field shape that minimizes variance in magnitude. From a thermal point of view, heat flows from the exit rings to the frame, which radiates to space and thermally conduct back to the mounting plate. The lateral screens allow the coils and the discharge chamber to radiate a portion of their heat. The frame carries structural loads and redistributes the heat. The magnetic components are bolted to the frame but do not carry any structural load. Finite element analysis shows the thruster design meets vibration requirements. The propellant isolator eliminates direct line of sight from high voltage to the ground of the propellant lines.

At the time of testing, the discharge channel of the test article was shaped in a way that approximated 3000 hours of wear based on the predictions of the Busek discharge channel wear model. Total duration of testing was

approximately 100 hours and the shape of the discharge channel was not expected to have change significantly over the that duration.

Table 1 shows the operating points tested during this facility effect characterization test. Operating points were selected to test a broad range of thruster usage, including potential low and high power settings. Electrical environment test was performed at OP1, OP4, OP5, and OP8 only.

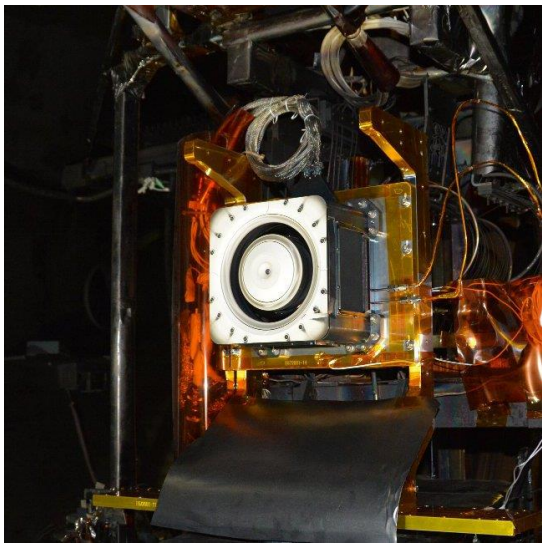

Fig. 1 BHT-6000 on VF5 thrust stand.

Table 1. Thruster operating points for this facility effect characterization test.

Operating Point	Discharge Voltage, V	Discharge Power, kW
OP1	300	3
OP2	300	4
OP3	300	4.5
OP4	300	5
OP5	600	3
OP6	600	4
OP7	600	5
OP8	600	6

B. Test Facility

Testing was performed in VF5 at NASA GRC. This cylindrical facility is 4.6 m in diameter, 18.3 m long, and was evacuated with a set of cryo-pumps. The thruster was mounted on a thrust stand located near one end of the facility with the thruster firing towards a beam dump at the other end. Fig. 2 shows the thruster installed in the VF5 test stand area and nearby test equipment. Fig. 3 shows the beam dump that the thruster fires into.

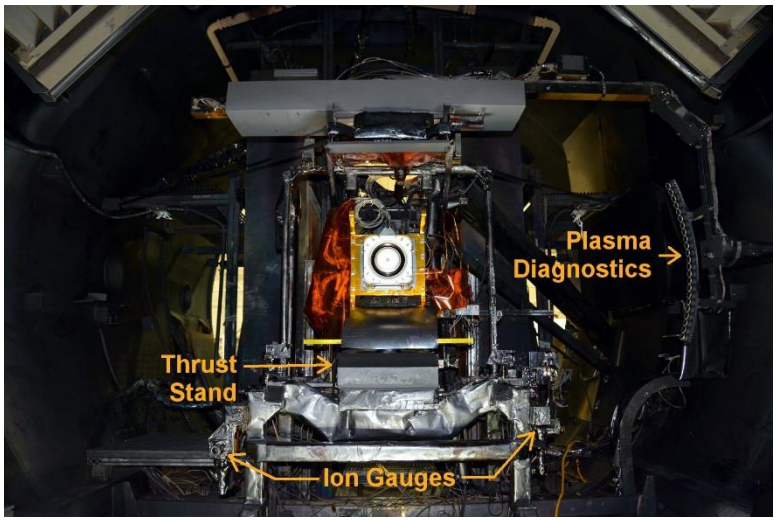

Fig. 2 Picture of the VF5 test stand area showing the locations of the thrust stand, plasma diagnostics, and ion gauges relative to the thruster.

Fig. 3 Picture of the VF5 beam dump that the thruster fires into.

Background pressure near the thruster was monitored with two ion gauges, which were calibrated on xenon against a spinning rotor gauge. Ion gauges were located approximately 1 m from the thruster and slightly upstream of the thruster exit plane. Ion gauge readings were corrected for temperature and direction relative to the background flux

via methods described in Yim and Burt [4]. Uncertainty in the calculated pressure was dominated by plasma-induced noise, electronic noise, and uncertainties associated with correction method. Total uncertainty in pressure measurement was estimated to be 10% to 15% of the reading. Background pressure was varied by injecting high purity xenon downstream of the thruster (approximately middle of the facility lengthwise). During the background pressure test, the background pressure near the thruster ranged from 1.5e-6 to 2.2e-5 Torr.

High purity xenon propellant was supplied via commercially available mass flow controllers to the anode and cathode. These mass flow controllers were calibrated using xenon prior to testing. Typical uncertainty of the calibrated measurements was ±1% of reading.

Electrical power was supplied to the thruster with commercially available power supplies. Separate power supplies powered the main discharge, cathode heater, keeper, and magnet. An electrical filter was placed between the thruster and the discharge power supply. All power supplies and the filter were located outside of the vacuum facility.

C. Diagnostics

Deployed diagnostics included a thrust stand and a set of plasma diagnostics on a two-axis probe arm. The plasma diagnostics included a Faraday probe (FP), a Langmuir probe (LP), a retarding potential analyzer (RPA), and a Wien filter spectrometer (WFS).

The thrust stand was tuned to maximize measurement resolution and minimize measurement uncertainty for the test article. Thermal drift in thrust measurements was corrected by using null coil measurement before and after hot fire operations when the thrust is known to be zero (i.e., no power going to the thruster and all propellant feed had been off for long enough for flow to be zero). For dedicated performance measurements, which occurred in the lowest background pressure with the beam dump electrically floating, zero-thrust measurements were taken before and after each operating point to minimize thrust uncertainty. For other tests, zero-thrust measurements were taken before and after groups of operations with varying background pressure or beam dump condition (e.g., OP1 operations at all tested background pressures was treated as a single group).

The use of a two-axis motion system allows positioning of the plasma diagnostics at various locations throughout the plume of the thruster. Fig. 2 shows the motion system located above the thruster; also shown are the plasma diagnostics mounted to the motion system probe arm. The motion system was aligned such that the axis of probe arm rotation (polar axis) passed through the firing axis of the thruster at the thruster exit plane. The distance (radial axis) of a plasma diagnostic from the thruster reported in this publication is measured from the axis of probe arm rotation to the collection surface of the diagnostic. Reported polar angle is defined as zero in the direction of the firing axis, positive to the right of the firing axis when viewing downstream, and negative to the left of the firing axis when viewing downstream. Faraday probe data was collected continuously while it swept arcs through the plasma plume. For all other plasma diagnostics, each diagnostic was moved to discrete locations for data collection. Offsets in position of the diagnostics were accounted for in the positioning. Positioning accuracy of the motion system was ±1 mm for the radial axis and ±0.2° for the polar axis.

The FP was of a guarded planar probe design [5] and was used to measure ion current density in the far-field plume. The angular resolution of the FP data was ~0.5°, limited by the size of the collector. For the background pressure test, the FP was swept at five radial distances with varying background pressures to provide the best extrapolation to zero pressure. The FP electrodes were biased at -30 V with respect to facility ground to repel electrons. For the electrical environment test, the FP was swept at 1000 and 1500 mm distance with different beam dump biases to characterize any change in the plume profile as the electrical environment changes. The FP electrodes were set to -30 V with respect to facility ground, except when the beam dump bias was negative the electrodes were set to beam dump bias minus 30 V (i.e., -35 V when beam dump bias was at -5 V, -50 V, when beam dump bias was at -20 V).

At polar angles of 30+ degrees from the firing axis, the FP was also used as a guarded Langmuir probe to provide high fidelity plasma potential and electron temperature measurements.

The LP was in the shape of a small disc and was used to measure plasma potential and electron temperature. The smaller size of the LP made it more appropriate for use in the densest part of the plasma plume, where the FP could not be used in Langmuir mode. For both the LP and the FP in Langmuir mode, approximately 6 ramps in bias voltage over 1 second was performed at each measurement location. The range of bias voltages swept by both the LP and the FP in Langmuir mode changed as the beam dump bias changed to properly capture both the ion and electron saturation regimes in each scan. For the background pressure test, Langmuir data was collected at 1500 mm distance and 5° interval from -105° to 105° from the firing axis except within 30° of the firing axis where 15° interval was used. For the electrical environment test, Langmuir data was collected at the same locations as the background pressure test as well as at a small subset of locations beyond 45° from the firing axis at 1000 mm distance.

The RPA was of an unaligned four-grid design based on an earlier design by the Air Force Research Laboratory [5] and was used to measure ion energy per charge distribution. This distribution was corrected by the plasma potential

measurements. During testing, the electron suppression and repelling grids were biased to -30 V with respect to facility ground. Data were obtained only during the background pressure test and were obtained at 5° interval from -105° to 105° from the firing axis except within 30° of the firing axis where 15° interval was used.

The WFS was a commercial product and was used to measure charged species current fractions. The electron suppression plate was biased at -30 V with respect to facility ground. Data were obtained only during the background pressure test and were obtained at 15° interval from -105° to 105° from the firing axis.

IV. Data Analysis and Uncertainties

Data analysis methods are essentially identical to recent methods used in other GRC tests [6-8] and are briefly described here.

Typically, a source of large uncertainty in thrust stand measurements is thermal drift. Using zero-thrust measurements, thermal drift was corrected assuming a linear trend over time. For reference, the zero-thrust value did not drift by more than 2 mN between measurements. Other sources of uncertainties were also analyzed according to methodology established in a prior publication [9], and the maximum thrust uncertainty was ±2.4 mN over the course of all tests. Maximum thrust uncertainty includes ±1 mN of systematic uncertainty while all other components were random. Specific impulse was calculated using thrust and total mass flow rate. The uncertainty in total mass flow rate was limited by the mass flow controllers to ±1%.

Ion current density data from the FP were analyzed by performing a standard set of corrections. The corrections include applying signal calibration, correction for ion current entering the gap between the collector and the guard, and correction for secondary electron emission from the FP due to impact of multiply-charged xenon ions. Then, linear curve-fits were made as functions of background pressure at different distances and angles to predict the ion current densities of the plume at zero pressure. Lastly, divergence angle and total beam current were calculated. Details of the FP analysis method including equations for divergence angle and total beam current can be found in a prior publication [7]. Uncertainty of the ion current density measurements were as low as ±5% at angles of less than 60° from the firing axis and grows to ±15% at 105° from the firing axis. Uncertainty in divergence angle is limited by FP collector size and alignment accuracy to ±0.5°. Uncertainty in the total beam current is driven by the main beam ion population and is within ±6%.

Langmuir data were corrected for signal calibration and then smoothed using Savitzky-Golay filters [10, 11]. Then the data were analyzed using simple Langmuir probe theory [12]. The measured plasma potentials were used to correct RPA data. Plasma potentials derived from Langmuir data had an overall uncertainty of ±4 V while electron temperatures had an overall uncertainty of ±50%.

RPA data was analyzed by correcting the bias voltage by the plasma potential and then smoothing the RPA trace using a Savitzky-Golay filter. Then, the negative of the derivative of the collector current with respect to the ion retarding grid bias voltage was taken. The result, plotted against the bias voltage, is proportional to the ion energy per charge distribution function [13]. The averaged ion energy per charge was calculated by averaging only the part of the trace where the amplitude exceeded half of the maximum amplitude. This approach is referred to as the threshold-based averaging with a 50% threshold. Based on prior studies, this approach provides a balance between excluding RPA-related artifacts and maintaining insensitivity to noise. Details of the RPA analysis method can be found in a prior publication [7]. Total uncertainty in the threshold-based averaged energy is ±10 eV, including the contributions from the plasma potential correction.

The WFS was used as a velocity filter to measure the ratio of charged species. Analysis of the data required accounting for changing transparency of the WFS as a function of bias voltage as well as correcting for charge exchange effect. The velocity distribution functions of each species were assumed to be skew-normal distributions, and appropriate transformation of the distributions for WFS transparency were made during curve-fitting. The resulting fits were numerically integrated to obtain the current fractions for the charged species. Details of the WFS analysis method can be found in prior publications [7, 14, 15]. Due to wide variability across operating points and polar angles, uncertainties for the current fractions were individually calculated and varied from a few percent near the firing axis to up to 50% outside of 60° from the firing axis. Methods for estimating the uncertainties in the current fractions can be found in a prior publication [14].

V. Results

A. Thruster Performance

Performance tests were performed on various days over the course of six weeks. The acquisition of zero-thrust measurements before and after each operating condition ensured that there were no biases in the data associated with

the order in which operating points were tested. In total, each of the eight operating points was tested six times. Each thrust measurement was processed as described in the Section IV and then corrected for discharge power using Eq. (1). Specific impulse was calculated from thrust and discharge-current-corrected total mass flow rate using Eqs. (2) and (3). For reference, the discharge power and discharge current were kept to within 1% of the target values. Averages and standard deviations across performance tests for each operating point were computed for the thrust and specific impulse. Standard error propagation was applied to compute the uncertainties in the thrust and specific impulse to 3-sigma confidence and included contributions from the measurement device uncertainties and spread in thruster behavior across tests. Performance tests were performed at the lowest achievable background pressure. Table 2 show a summary of the averages and 3-sigma uncertainties for the thrust and specific impulse as well as background pressure for each operating point.

$$Thrust_{Corrected} = Thrust_{Measured} * \frac{Target\ discharge\ power}{Discharge\ power} \tag{1}$$

$$Specific\ Impulse_{Corrected} = \frac{Thrust_{Corrected}}{g_0 * Total\ mass\ flow\ rate_{Corrected}} \tag{2}$$

$$Total\ mass\ flow\ rate_{Corrected} = Total\ mass\ flow\ rate_{Measured} * \frac{Target\ discharge\ current}{Discharge\ current} \tag{3}$$

Table 2. Summary of performance test results.

Operating Point	Discharge Voltage, V	Discharge Power, kW	Background Pressure, μT	Averaged thrust, mN	Uncertainty, thrust, 3-σ, mN	Averaged specific impulse, s	Uncertainty, specific impulse, 3-σ, s
OP1	300	3	2.7	191.4	±2.4	1794	±37
OP2	300	4	3.4	249.5	±2.2	1855	±35
OP3	300	4.5	3.8	276.6	±2.4	1878	±34
OP4	300	5	4.1	302.4	±2.4	1898	±36
OP5	600	3	1.5	133.8	±4.1	2176	±57
OP6	600	4	1.9	181.9	±4.1	2271	±48
OP7	600	5	2.4	228.9	±4.2	2354	±43
OP8	600	6	2.8	285.7	±4.4	2485	±53

B. Background pressure characterization

During background pressure test at each operating point, the thruster was tested at the lowest achievable background pressure, then approximately two times, three times, and five times the lowest achievable background pressure, in that order. Mass flow rates were adjusted to maintain the discharge current needed for each operating point. Fig. 4 and Fig. 5 show the change in thrust and specific impulse, respectively, compared to the values at the lowest achievable background pressure as functions of background pressure.

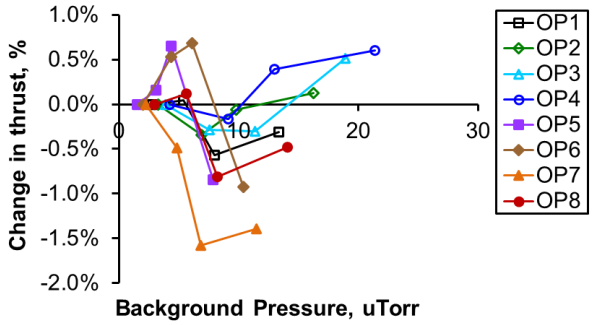

Fig. 4 Change in thrust with background pressure.

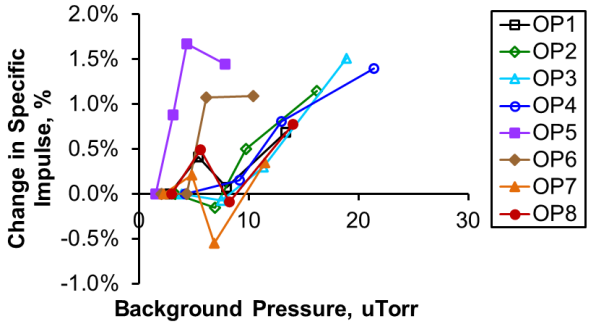

Fig. 5 Change in specific impulse with background pressure.

With the exception of OP7, thrust changed by no more than ±1% over the tested background pressures. Specific impulse generally increased with background pressure. This trend can be explained by the fact that the thruster required less supplied mass flow (i.e., ingested more flow from the background) while producing the same thrust as the background pressure increased. Extrapolating the data to zero pressure via linear fits shows that the predicted performance at zero pressure differed from values at the lowest achievable pressure by less than 1% for all operating points. This amount of difference is on the order of or less than the measurement uncertainties in Table 2.

Fig. 6 and Fig. 7 show the ion current density profiles for OP4 and OP8, respectively, 1 m from the thruster and at different background pressures. Background pressures are labeled as multiples of the lowest achievable pressure (e.g., "P3x" corresponds to three times the lowest achievable pressure). Also shown are the predicted zero-pressure profiles (labeled "P0x") obtained by performing linear curve-fits against background pressure at each polar angle.

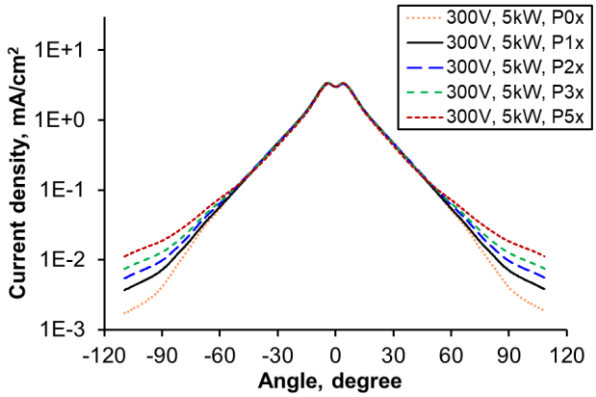

Fig. 6 Ion current density profile for OP4 at 1 m from the thruster and various background pressures.

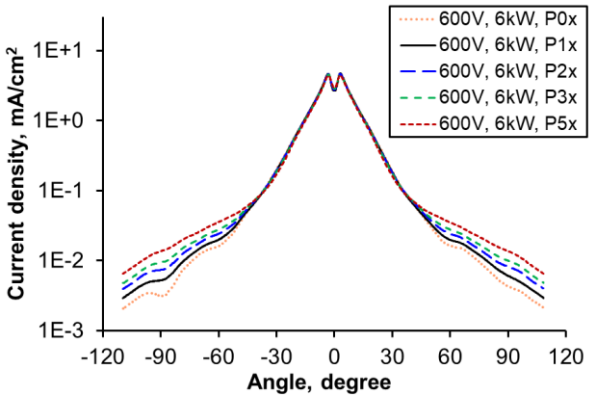

Fig. 7 Ion current density profile for OP8 at 1 m from the thruster and various background pressures.

From Fig. 6 and Fig. 7, one can see that the current density of the main beam within ±45° of the firing axis does not vary over the tested range of pressures to within measurement uncertainty. Beyond 45° from the firing axis, the magnitude of current density decreases as the background pressure decreases, and the shape of the profile changes enough to reveal distinctive structures. In particular, for OP8, one can observe two distinct populations, one centered at ~70° and the other centered at ~95° from the firing axis. In other words, as the background pressure increased, otherwise distinct ion populations were smeared out over polar angle and became indistinct. The aforementioned trends are likely result of charge exchange interactions between the plume and the background neutrals. Since background neutrals have little directional kinetic energy and much random kinetic energy, they have large divergence. When charge exchange occurs between beam ions and background neutral, the resulting slow ion will have large divergence and will appear to smear out the plume current density profile. Similar behavior has been observed in Hall thrusters as reported in other publications [7, 16, 17]. Another interesting observation is the presence of low-density populations beyond 60° from the firing axis of the thruster. These populations may be related to recently identified side plume ions in magnetically-shielded Hall thrusters [18], though it should be noted that during this test the discharge channel of the BHT-6000 had a shape that approximated 3000 hours of wear, which is not the same as the near-zero-erosion shape seen in magnetically-shielded thrusters.

Table 3 lists the calculated divergence angle and total beam current for various operating points at the tested background pressures. Divergence angles and total beam currents calculated from the predicted zero-pressure profiles are also shown.

Table 3. Summary of divergence angle and total beam current for the background pressure test.

Operating Point	Discharge Voltage, V	Discharge Power, kW	Background Pressure, μT	Divergence angle, deg.	Total beam current, A
OP1	300	3	0	27.3	8.73
			2.7	26.9	8.66
			5.3	26.4	8.69
			8.1	26.0	8.64
			13.4	25.3	8.58
OP2	300	4	0	28.1	11.61
			3.5	27.7	11.56
			6.8	26.9	11.55
			10.0	26.6	11.56
			16.6	26.0	11.49
OP3	300	4.5	0	28.6	13.06
			3.8	28.3	13.09
			7.6	27.4	12.92
			11.3	26.9	13.01
			18.7	26.4	12.95
OP4	300	5	0	29.1	14.40
			4.2	28.6	14.29
			8.9	28.2	14.48
			12.9	27.4	14.52
			21.4	26.8	14.35
OP5	600	3	0	24.7	4.10
			1.6	24.4	4.10
			3.2	25.5	3.98
			4.6	25.5	3.99
			7.8	25.2	3.93
OP6	600	4	0	23.7	5.54
			2.0	24.0	5.50
			4.3	22.9	5.49
			6.1	23.5	5.50
			10.1	23.4	5.42
OP7	600	5	0	22.7	6.95
			2.4	22.6	6.90
			4.7	22.7	6.92
			6.9	22.5	6.89
			11.7	22.5	6.85
OP8	600	6	0	23.8	9.10
			2.8	23.6	9.06
			5.6	23.6	9.09
			8.2	23.5	9.09
			14.0	23.1	9.02

Fig. 8 shows the difference in the divergence angle from the zero-pressure value as a function of background pressure for all tested operating points. Note this figure shows the absolute value of the difference. Operations at 300 V discharge voltage exhibited greater variation in divergence angle with background pressure than operations at 600 V, particularly at pressures greater than 10 μTorr. Based on the data presented, high accuracy measurements of current density profiles require background pressures in the single digit μTorr or less.

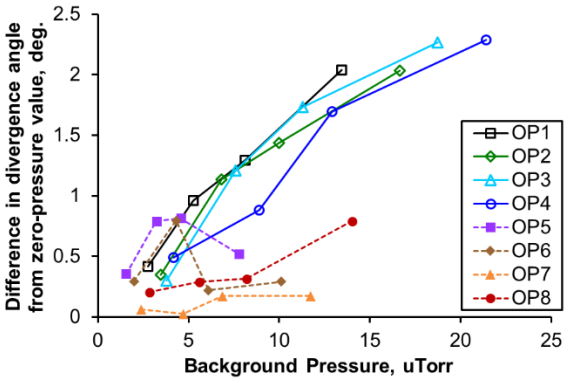

Fig. 8 Difference in divergence angle from zero-pressure value versus background pressure.

Fig. 9 shows ion energy per charge distribution for OP4 at a location of -90° from the firing axis and 1.5 m from the thruster over the tested background pressures. Fig. 10 shows the same for OP8 at a location of -60° from the firing axis. In these figures, the y-axis is on a log scale and small apparent differences in the y-direction represent large differences on an absolute scale. Also in these figures are dotted horizontal lines indicating the noise floor below which the points shown are likely to be noise. The noise floor is defined as three times the standard deviation of the data in the region that should contain only noise (defined as > 800 eV in this data set).

From Fig. 9 and Fig. 10, one can see that there are measurable differences in the ion energy per charge profiles as the background pressure varied. In particularly, low-energy (<50 eV) population increases in quantity as the background pressure increases, which can be attributed to charge-exchange actions directing slow ions to the sides of the thruster plume. A medium-energy (100-200 eV) population present during 600 V operations increase in energy as the background pressure decreases. A possible mechanism for this was described in a prior work [18]. Beam-energy (energy near discharge voltage) population for 300 V operations decreases in quantity as the background pressure increases, which can also be attributed to charge-exchange actions. Interestingly, the quantity of beam-energy population for 600 V operations appeared to remain constant with changing pressure.

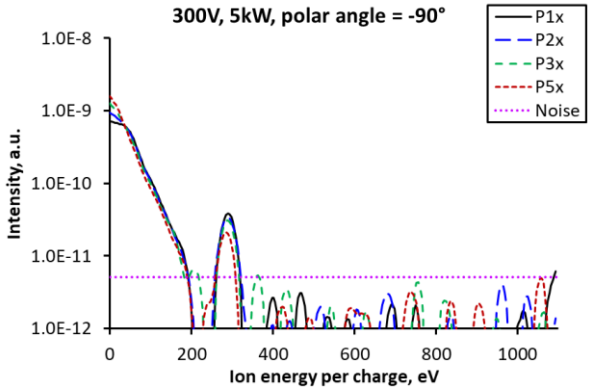

Fig. 9. Ion energy per charge distribution for OP4 at a location of -90° from the firing axis and 1.5 m from the thruster over the tested pressures.

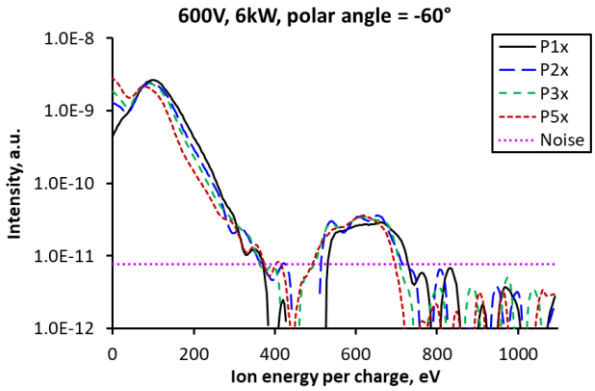

Fig. 10 Ion energy per charge distribution for OP8 at a location of -60° from the firing axis and 1.5 m from the thruster over the tested pressures.

Table 4 lists the ion energy per charge of beam ions for various operating points at the tested background pressures. In this table, pressure is listed as multiples of lowest achievable background pressures. Actual pressure values can be found in Table 3. In this table, ion energy per charge was averaged over ±15° from firing axis, within which ions were found to consist of only beam energy ions for all operating points. Results in this table show that ion energy per charge of the beam ions were consistent across background pressure and discharge power (for a given discharge voltage). Based on the data presented, accurate energy measurements of the beam population can be performed at the high end of the tested background pressures (~20 μTorr). However, density measurements and measurements of low to medium energy ion populations can only be made accurately at less than a few μTorr. Additional RPA data in the form of normalized ion energy per charge distributions versus polar angles at the lowest achieved background pressure can be found in the Appendix Fig. 23 to Fig. 30.

Table 4. Summary of ion energy per charge of beam ions for the background pressure test.

	Ion energy per charge of beam ions, eV							
Pressure	**OP1**	**OP2**	**OP3**	**OP4**	**OP5**	**OP6**	**OP7**	**OP8**
P1x	283.8	281.6	281.3	281.0	585.2	585.0	583.3	577.8
P2x	282.2	280.6	280.4	278.7	584.6	583.2	583.1	577.5
P3x	280.5	279.6	279.8	278.2	584.1	583.6	583.5	577.4
P5x	278.9	277.6	278.4	276.7	583.5	583.7	583.0	575.5

Fig. 11 and Fig. 12 show normalized spectra from the WFS at different background pressures for OP4 and OP8, respectively. Fig. 11 shows that the ratios of multiply-charged species to singly-charged species increase with background pressure and this trend was present for all 300 V operations. Fig. 12 shows that the ratios of species were approximately constant over the tested background pressure and this trend was present for all 600 V operations. Note that the presented figures are without corrections for charge exchange. Data after correction for charge exchange that are presented later in the paper show the same trends.

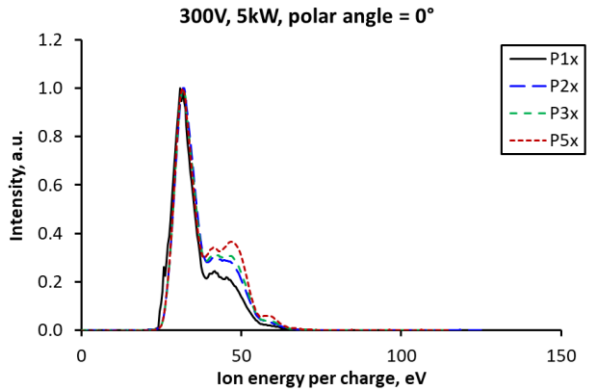

Fig. 11 Normalized WFS spectra at different background pressures for OP4.

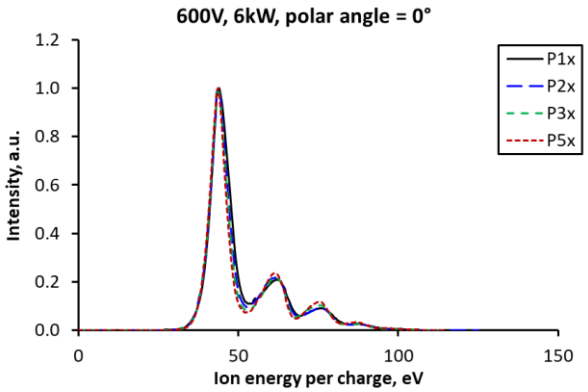

Fig. 12 Normalized WFS spectra at different background pressures for OP8.

Table 5 and Table 6 show the main beam current fractions over all tested pressures for OP1 to OP4 (300 V discharge) and OP5 to OP8 (600 V discharge), respectively. Data in these tables were obtained at a polar angle of 0° to ensure only main beam plasma was measured.

Table 5. Summary of main beam current fractions for OP1 to OP4.

	OP1			OP2			OP3			OP4		
Pressure	**Xe^+**	**Xe^{2+}**	**Xe^{3+}**	**Xe^+**	**Xe^{2+}**	**Xe^{3+}**	**Xe^+**	**Xe^{2+}**	**Xe^{3+}**	**Xe^+**	**Xe^{2+}**	**Xe^{3+}**
P1x	0.794	0.155	0.051	0.743	0.239	0.018	0.727	0.273	0.000	0.709	0.183	0.108
P2x	0.792	0.145	0.063	0.733	0.237	0.030	0.710	0.197	0.093	0.703	0.259	0.038
P3x	0.778	0.147	0.075	0.728	0.223	0.049	0.699	0.231	0.070	0.694	0.281	0.026
P5x	0.769	0.143	0.088	0.708	0.237	0.055	0.694	0.260	0.046	0.679	0.262	0.059

Table 6. Summary of main beam current fractions for OP5 to OP8.

	OP5			OP6			OP7			OP8		
Pressure	**Xe^+**	**Xe^{2+}**	**Xe^{3+}**	**Xe^+**	**Xe^{2+}**	**Xe^{3+}**	**Xe^+**	**Xe^{2+}**	**Xe^{3+}**	**Xe^+**	**Xe^{2+}**	**Xe^{3+}**
P1x	0.721	0.221	0.058	0.726	0.209	0.064	0.702	0.219	0.079	0.682	0.242	0.076
P2x	0.733	0.205	0.061	0.725	0.205	0.070	0.711	0.211	0.077	0.680	0.244	0.075
P3x	0.739	0.197	0.063	0.733	0.194	0.073	0.725	0.198	0.077	0.691	0.223	0.086
P5x	0.753	0.181	0.066	0.734	0.192	0.075	0.723	0.196	0.081	0.698	0.217	0.085

WFS data taken in the side plume of the thruster were generally inconclusive due to the presence of more than one ion population that overlap with each other. Fig. 13 shows example WFS traces at various polar angles for OP4. Traces were divided into two subplots for clarity. Within 60° of the firing axis, WFS spectra were reasonably resolved (i.e., can be analyzed by curve fitting) with spectra from higher angles being generally less broad than spectra near the firing axis. At 75+° from the firing axis, low energy population began to appear that complicated analysis.

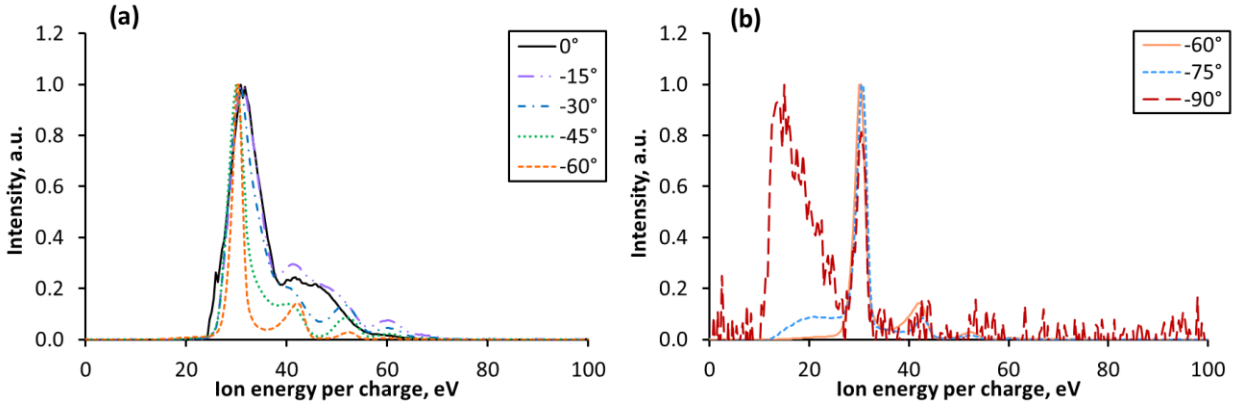

Fig. 13 Normalized WFS spectra for OP4 at various polar angles.

Fig. 14 shows example WFS traces at various polar angles for OP8. Traces were divided into two subplots for clarity. Whereas a low energy population was visible in the spectra at 75+° for 300 V operations, low and medium energy populations were visible in the spectra at 45+° for 600 V operations. This trend may be related to the fact that beam ions are less divergent for 600 V operations and lower energy ions become relatively easier to detect. Another possibility is that there were more lower energy ions present during 600 V operations than 300 V operations.

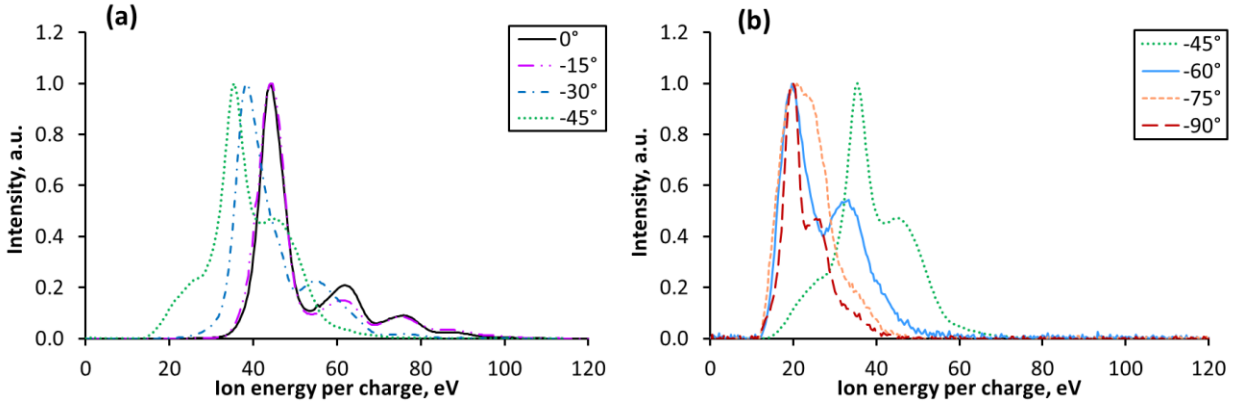

Fig. 14 Normalized WFS spectra for OP8 at various polar angles.

C. Electrical environment characterization

Electrical environment tests were performed by biasing the beam dump in VF5. First, the beam dump voltage was ramped from -20 to +60 with respect to the facility ground (specifically, -20, -10, -5, 0, 5, 10, 15, 20, 40, and 60 V, in order) and the thruster dwelled for about five minutes at each step. Then, the beam dump bias was set to +60, +20, -5, and -20 V, in order, and probe data were taken at each of these four voltage settings. Only OP1, OP4, OP5, and OP8 were tested. Note that beam dump voltage ramping occurred over seconds per step, during which the data acquisition system continuously recorded telemetry at a rate of ~5 Hz. Data points seen in subsequent figures with beam dump bias voltage between the aforementioned discrete voltages resulted from the slow ramping.

Fig. 15 and Fig. 16 show changes in thrust and beam dump current, respectively, as functions of the beam dump bias voltage during the bias voltage ramp-up of the electrical environment test for the tested operating points. In Fig. 15, with the exception of occasional outliers, thrust data differed from the average thrust by less than the measurement uncertainty of the thrust stand for all tested operating points. Operation of the thruster appeared to not have been affected by variations in the beam dump bias voltage. In Fig. 16, the plot of beam dump current versus beam dump

bias voltage exhibited the appearance of a Langmuir probe trace [12]. This is an indication that the beam dump acted as a large Langmuir probe on the plume of the thruster. The fact the current was nearly constant as a function of voltage in the saturation regions (both ion and electron saturation) indicates minimal coupling between the beam dump and the thruster. This data provides verification that the centrally mounted cathode coupled well to the thruster plume and was not coupling to the rest of the facility. In Fig. 16, the magnitude of the ion saturation current of OP8 was larger than that of OP1 despite the two operating point having the same discharge current because the current density profile of OP8 is more convergent than OP1 (i.e., more of the beam current landed on the beam dump for OP8 than for OP1). In contrast, the magnitude of electron saturation current was the same for OP1 and OP8 because the two operating points had the same discharge current.

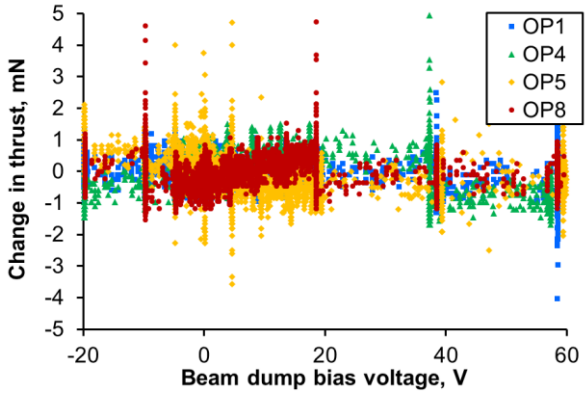

Fig. 15 Change in thrust as the beam dump bias varied for the tested operating points.

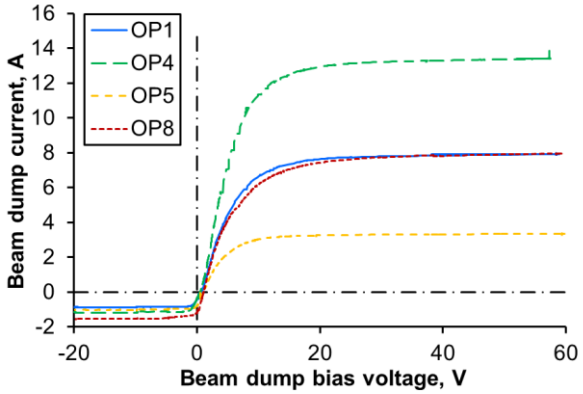

Fig. 16 Beam dump current as the beam dump bias voltage varied for the tested operating points.

Fig. 17 and Fig. 18 show the ion current density profiles for OP4 and OP8, respectively, 1 m from the thruster and at different beam dump biases. The current density profiles were essentially identical across beam dump biases. Slight differences were detected at the sides (~90° from firing axis) for the highest positive bias voltage of 60 V, but the magnitude was on the order of the measurement uncertainty.

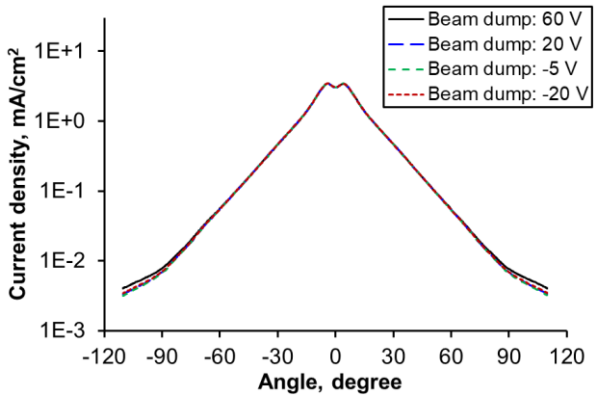

Fig. 17 Ion current density profile for OP4 at 1 m from the thruster and various beam dump biases.

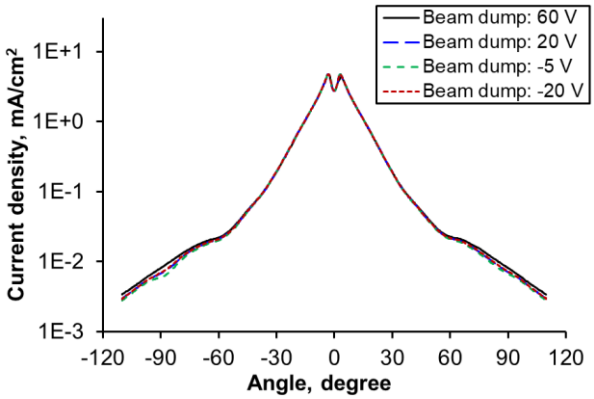

Fig. 18 Ion current density profile for OP8 at 1 m from the thruster and various beam dump biases.

Fig. 19 and Fig. 20 show the plasma potential for OP4 and OP8, respectively, 1.5 m from the thruster and at different beam dump biases. Since the beam dump bias is driving the cathode potential for the entire plasma circuit, it can be difficult to discern whether there were real changes in the plasma potential as the beam dump bias varied. To gain better insight, cathode potential is subtracted from the plasma potential, and the result plotted in Fig. 21 and Fig. 22 for OP4 and OP8, respectively. In other words, instead of calculating the plasma potential against the facility ground (plasma diagnostics make measurements against facility ground), the plasma potential is calculated against the cathode potential. Note that Langmuir probe traces were obtained at 1 m distance but at a coarser angular resolution; the 1.5-m data set is more comprehensive for the purpose of detailed examinations.

From Fig. 21 and Fig. 22, one can see that the plasma potential profiles were largely constant over different beam dump bias voltages, with the notable exception of OP8 at beam dump bias voltage of 60 V. Probe data were especially noisy at OP8 and the difference in plasma potential profile at 60 V versus the other beam dump bias voltage may be an artifact of the noise in the probe data. A possible hypothesis for the increase in noise was that the plasma potential being at ~60 V combined with energetic electrons from the thruster may have enabled sporadic micro-arcs to form on the probe collection surfaces. Note that the facility side walls sat at facility ground potential. Excepting the aforementioned possible artifact, the data indicate that the thruster maintained the same plasma potential profile as the beam dump bias voltage varied.

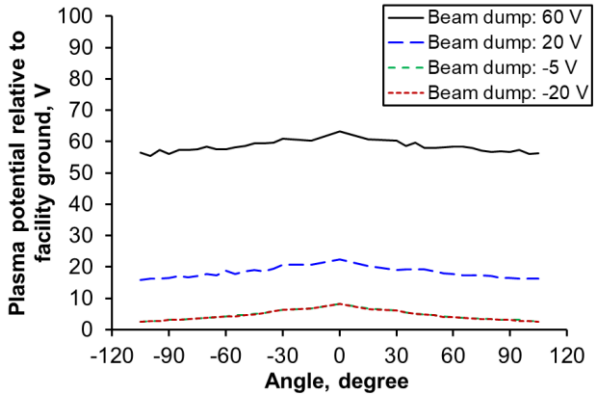

Fig. 19 Plasma potential relative to facility ground for OP4 at 1.5 m from the thruster and various beam dump biases.

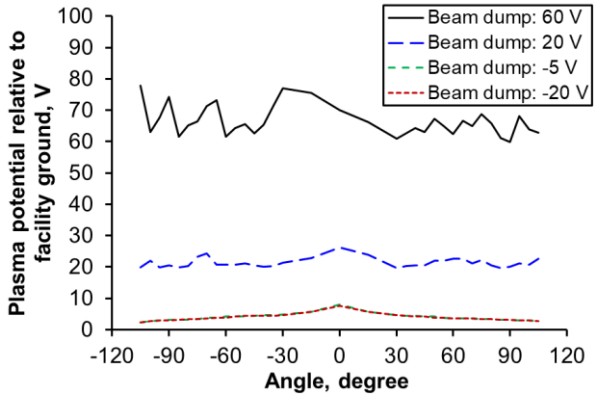

Fig. 20 Plasma potential relative to facility ground for OP8 at 1.5 m from the thruster and various beam dump biases.

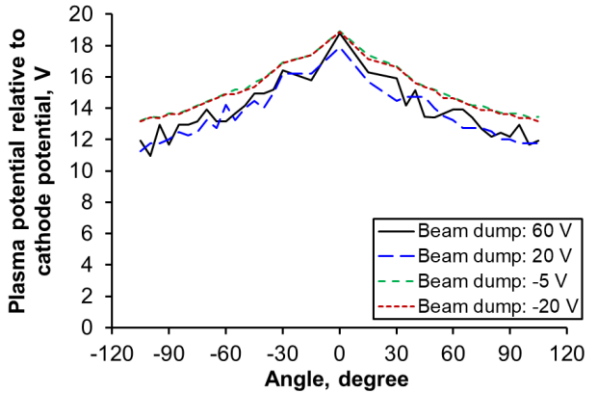

Fig. 21 Plasma potential relative to cathode potential for OP4 at 1.5 m from the thruster and various beam dump biases.

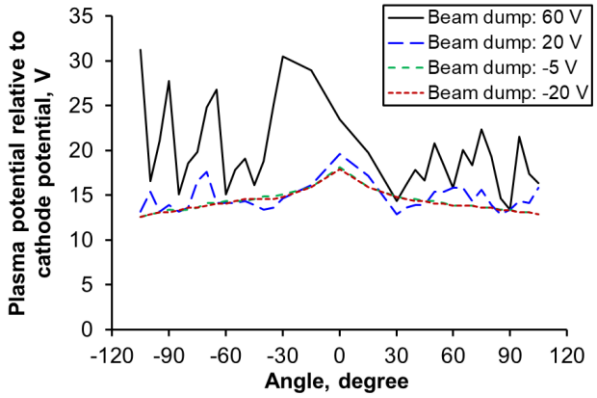

Fig. 22 Plasma potential relative to cathode potential for OP8 at 1.5 m from the thruster and various beam dump biases.

VI. Conclusions

A series of facility effect tests were completed with the BHT-6000 in VF5. Results established a set of performance benchmarks to high level of accuracy to support mission design for the flight of PPE. During the background pressure test, the thrust was found to be constant to within measurement uncertainty over the tested range of pressures. Specific impulse was found to increase slightly (1 to 1.5%) with increasing pressure (up to 20 μTorr depending on operating point).

With the exception of select quantities (e.g., ion energy of beam ions), plume properties in a space-like environment can only be predicted accurately from measurements taken at <10 μTorr and often required extrapolations from measurements at multiple background pressures. Properties of the side plume (approximately greater than 45° from the firing axis) were particularly sensitive to background pressures and the values of some properties only became space-like at less than a few μTorr. These results are similar to findings from other background pressure studies [7, 19].

Electrical environment test results showed that the BHT-6000 operated identically with changing beam dump bias voltage to within measurement uncertainty. An issue with plasma potential data when the thruster was operated at 600 V, 6 kW with beam dump bias of 60 V was likely due to artifacts in the probe measurement.

Appendix

Fig. 23 to Fig. 30 show plots of normalized ion energy per charge distribution versus polar angles for all operating points at their respective lowest achieved background pressure.

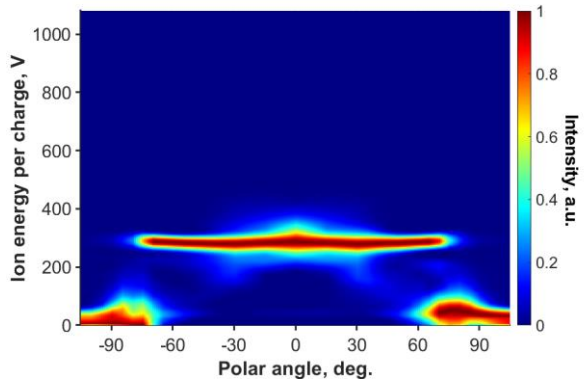

Fig. 23 Normalized ion energy per charge distribution versus polar angles for OP1.

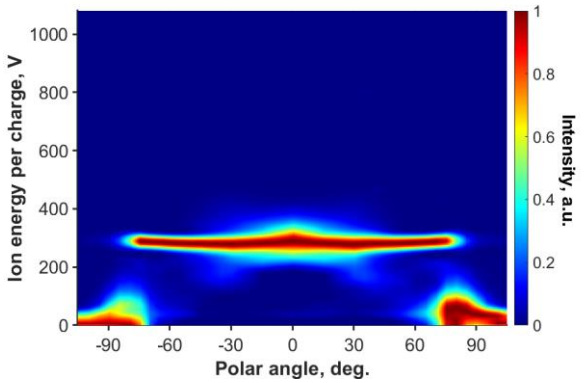

Fig. 24 Normalized ion energy per charge distribution versus polar angles for OP2.

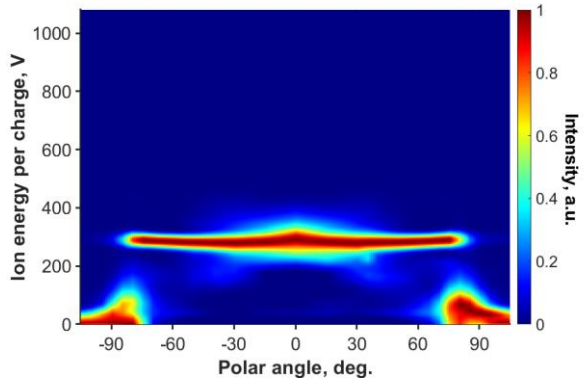

Fig. 25 Normalized ion energy per charge distribution versus polar angles for OP3.

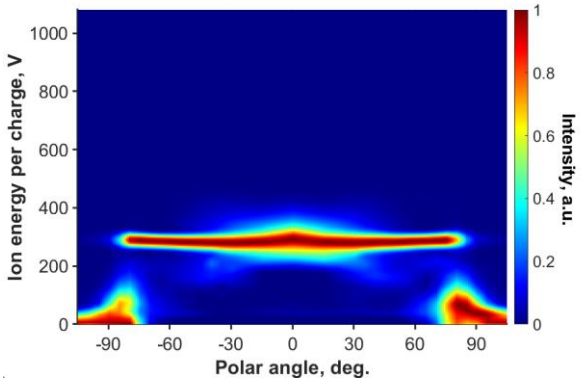

Fig. 26 Normalized ion energy per charge distribution versus polar angles for OP4.

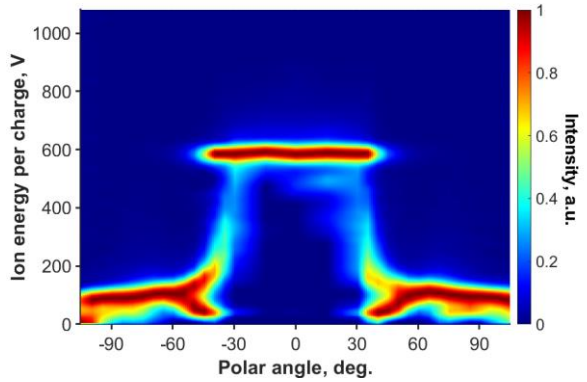

Fig. 27 Normalized ion energy per charge distribution versus polar angles for OP5.

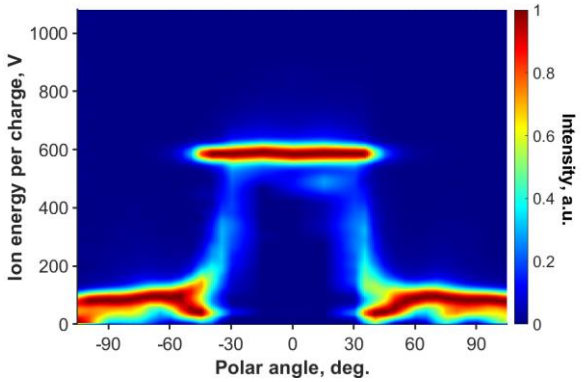

Fig. 28 Normalized ion energy per charge distribution versus polar angles for OP6.

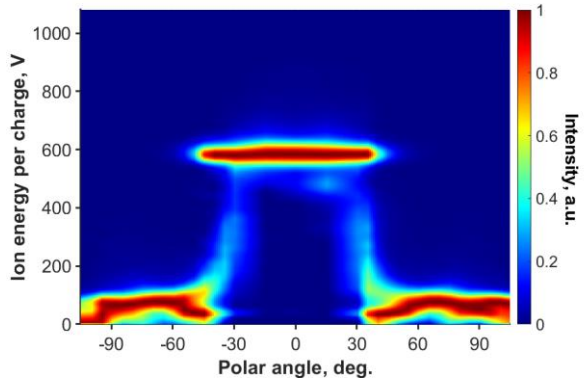

Fig. 29 Normalized ion energy per charge distribution versus polar angles for OP7.

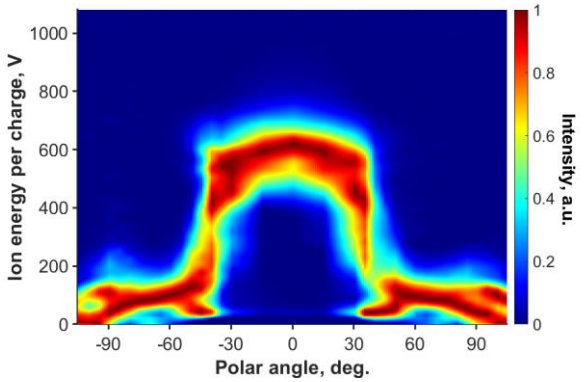

Fig. 30 Normalized ion energy per charge distribution versus polar angles for OP8.

Acknowledgments

The authors would like to thank the NASA Exploration Systems Development Mission Directorate for funding this work. The authors would like to thank David T. Jacobson of NASA and Ron Corey of Maxar Space Systems for technical leadership. The authors would like to thank Dionne M. Hernandez-Lugo of NASA and Taylor Winkelmann of Maxar Space Systems for managing the work.

The authors would like to thank Kevin L. Blake, Matthew T. Daugherty, Douglas A. Edsey, Jason D. Frieman, Joshua D. Gibson, Timothy G. Gray, Chad E. Joppeck, Jon A. Mackey, Robert J. Makovec, Kevin J. Rahill, Corey R. Rhodes, Trish Seaman, Richard G. Senyitko, Luke Sorrelle, George C. Soulas, James M. Szelagowski, and John T. Yim of NASA, David Cooper and Peter Zollinger of Maxar Space Systems, and Ryan Fagan of Busek Co. Inc. for work on test preparations and test operations.

References

[1] Fuller, S., Lehnhardt, E., Connell, D., Zaid, C., and Halloran, K., "Gateway Program Status and Overview", *International Astronautical Congress*, NTRS-20220013534, Paris, Sep 1, 2022.

[2] Herman, D. A., Gray, T. G., Johnson, I., Hussein, S., and Winkelmann, T., "Development and Qualification Status of the Electric Propulsion Systems for the NASA PPE Mission and Gateway Program", *International Electric Propulsion Conference 2022*, 2022-465, Boston, MA, Jun 19-23, 2022.

[3] Mullins, C., Hruby, V., Pote, B., Blake, K., and Lenguito, G., "Development of a 5kW Class Hall Thruster", *36th International Electric Propulsion Conference*, 2019-492, Vienna, Austria, Sep 15-20, 2019.

[4] Yim, J. T. and Burt, J. M., "Characterization of Vacuum Facility Background Gas Through Simulation and Considerations for Electric Propulsion Ground Testing", *51st AIAA/SAE/ASEE Joint Propulsion Conference*, AIAA-2015-3825, Orlando, FL, Jul 27-29, 2015. https://doi.org/10.2514/6.2015-3825

[5] Huang, W., Shastry, R., Soulas, G. C., and Kamhawi, H., "Farfield Plume Measurement and Analysis on the NASA-300M and NASA-300MS", *33rd International Electric Propulsion Conference*, 2013-057, Washington, DC, Oct 6-10, 2013.

[6] Kamhawi, H., Huang, W., Haag, T. W., Yim, J. T., Herman, D. A., Peterson, P. Y., Williams, G. J., Gilland, J. H., Hofer, R. R., and Mikellides, I. G., "Performance, Facility Pressure Effects, and Stability Characterization Tests of NASA's Hall Effect Rocket with Magnetic Shielding Thruster", *52nd AIAA/SAE/ASEE Joint Propulsion Conference*, AIAA-2016-4826, Salt Lake City, UT, Jul 25-27, 2016. https://doi.org/10.2514/6.2016-4826

[7] Huang, W., Kamhawi, H., Haag, T. W., Lopez Ortega, A., and Mikellides, I. G., "Facility Effect Characterization Test of NASA's HERMeS Hall Thruster", *52nd AIAA/SAE/ASEE Joint Propulsion Conference*, AIAA-2016-4828, Salt Lake City, UT, Jul 25-27, 2016. https://doi.org/10.2514/6.2016-4828

[8] Huang, W., Williams, G. J., Peterson, P. Y., Kamhawi, H., Gilland, J. H., and Herman, D. A., "Plasma Plume Characterization of the HERMeS during a 1722-hr Wear Test Campaign", *35th International Electric Propulsion Conference*, 2017-307, Atlanta, GA, Oct 8-12, 2017.

[9] Mackey, J. A., Haag, T. W., Kamhawi, H., Hall, S. J., and Peterson, P. Y., "Uncertainty in Inverted Pendulum Thrust Measurements", *NASA Technical Memorandum*, TM-2018-219952, Washington, D.C., Aug, 2018.

[10] Savitzky, A. and Golay, M. J. E., "Smoothing and Differentiation of Data by Simplified Least Squares Procedures", *Analytical Chemistry*, Vol. 36, No. 8, Jul, 1964, pp. 1627-1639. https://doi.org/10.1021/ac60214a047

[11] Steinier, J., Termonia, Y., and Deltour, J., "Comments on Smoothing and Differentiation of Data by Simplified Least Squares Procedure", *Analytical Chemistry*, Vol. 44, No. 11, Sep, 1972, pp. 1906-1909. https://doi.org/10.1021/ac60319a045

[12] Lieberman, M. A. and Lichtenberg, A. J., "Electrostatic Probe Diagnostics," in *Principles of Plasma Discharges and Materials Processing*, 2nd ed., Wiley, New York, 2005, pp. 185-203. https://doi.org/10.1002/0471724254

[13] Hutchinson, I. H., *Principles of Plasma Diagnostics*, 2nd ed., Cambridge University Press, 2002. https://doi.org/10.1017/CBO9780511613630

[14] Huang, W. and Shastry, R., "Analysis of Wien filter spectra from Hall thruster plumes", *Review of Scientific Instruments*, Vol. 86, No. 7, Jul 6, 2015, pp. 073502. https://doi.org/10.1063/1.4923282

[15] Shastry, R., Hofer, R. R., Reid, B. M., and Gallimore, A. D., "Method for analyzing ExB probe spectra from Hall thruster plumes", *Review of Scientific Instruments*, Vol. 80, No. 6, Jun 22, 2009, pp. 063502. https://doi.org/10.1063/1.3152218

[16] Diamant, K. D., Liang, R., and Corey, R. L., "The Effect of Background Pressure on SPT-100 Hall Thruster Performance", *50th AIAA/ASME/SAE/ASEE Joint Propulsion Conference*, AIAA-2014-3710, Cleveland, OH, Jul 28-30, 2014. https://doi.org/10.2514/6.2014-3710

[17] Diamant, K. D., Curtiss, T. J., Spektor, R., Beiting, E. J., Hruby, V., Pote, B., Kolencik, J., and Paintal, S., "Performance and Plume Characterization of the BHT-1500 Hall Thruster", *34th International Electric Propulsion Conference*, 2015-069, Kobe, Japan, Jul 4-10, 2015.

[18] Huang, W. and Kamhawi, H., "The Side Plume of Magnetically Shielded Hall Thrusters", *International Electric Propulsion Conference 2022*, 2022-402, Boston, MA, Jun 19-23, 2022.

[19] Huang, W., Kamhawi, H., and Haag, T. W., "Effect of Background Pressure on the Performance and Plume of the HiVHAc Hall Thruster", *33rd International Electric Propulsion Conference*, 2013-058, Washington, DC, Oct 6-10, 2013.